Biochemistry and Biophysics Reports 24 (2020) 100827

Contents lists available at ScienceDirect

Biochemistry and Biophysics Reports

journal homepage: www.elsevier.com/locate/bbrep

Interaction of synthetic antimicrobial peptides of the Hylin a1 family with models of eukaryotic structures: Zwitterionic membranes and DNA

Gabriel S. Vignoli Muniz [a,*], Lilia I. De la Torre [b], Evandro L. Duarte [a], Esteban N. Lorenzón [c], Eduardo M. Cilli [d], Andrea Balan [b], M. Teresa Lamy [a,**]

[a] Instituto de Física, Universidade de São Paulo, SP, Brazil
[b] Instituto de Ciências Biomédicas, Universidade de São Paulo, SP, Brazil
[c] Unidade Acadêmica Especial Ciências da Saúde, Universidade Federal de Jataí, Jataí, GO, Brazil
[d] Instituto de Química, Universidade Estadual Paulista, Araraquara, SP, Brazil

ARTICLE INFO

Keywords:
Antimicrobial peptides
DPPC vesicles
DNA
DSC
Fluorescence spectroscopy
Electrophoresis

ABSTRACT

Antimicrobial peptides (AMPs) have been appointed as a possible alternative to traditional antibiotics in face of pathogens increasing resistance to conventional drugs. Hylin a1 (IFGAILPLALGALKNLIK), an AMP extracted from the skin secretion of a South American frog, *Hypsiboas albopunctatus*, was found to show a strong cytotoxicity against bacteria and fungus, but also a considerable hemolytic action. Considering the toxicity of the peptide in eukaryotic cells, this work focuses on investigating the effects of the interaction of the Hylin a1 analogues W^6Hya1, D^0W^6Hya1 and K^0W^6Hya1 with models of eukaryotic structures, namely zwitterionic liposomes of dipalmitoyl phosphatidylcholine (DPPC) and calf-thymus DNA (CT DNA). Through intrinsic Trp fluorescence we determined that the peptide affinity for fluid DPPC bilayers follows the decreasing order: D^0W^6Hya1 (+2) > W^6Hya1 (+3) » K^0W^6Hya1 (+4). Fluorescence data also indicate that the Trp residue in the more positively charged peptide, K^0W^6Hya1, is less deep in the bilayer than the residue in the other two peptides. This finding is supported by differential scanning calorimetry (DSC) data, which shows that both D^0W^6Hya1 and W^6Hya1 disturb DPPC gel-fluid transition slightly more effectively than K^0W^6Hya1. DPPC DSC profiles are homogeneously disturbed by the three peptides, probably related to peptide-membrane diffusion. Surprisingly, the peptide that displays the lowest affinity for PC membranes and is located at the more superficial position in the bilayer, K^0W^6Hya1, is the most efficient in causing formation of pores on the membrane, as attested by carboxyfluorescein leakage assays. The three peptides were found to interact with CT DNA, with a deep penetration of the Trp residue into hydrophobic pockets of the double helix, as indicated by the significant blue shift on the Trp fluorescence, and the displacement of DNA-bound ethidium bromide by the peptides. The experiments of DNA electrophoresis confirm that Hylin peptides bind DNA in a concentration-dependent manner, inducing complete DNA retardation at the relative AMP/plasmid DNA weight ratio of ~17. These findings could help to better understand the AMPs toxic effects on eukaryotic cells, thus contributing to the design of healthier therapeutic agents.

1. Introduction

Due to the increasing resistance of pathogens against traditional antibiotics, as well as the emergence of new diseases, a severe and relevant threat to public health on a global scale, the scientific community has been making efforts in search for new therapeutic drugs [1–3]. Among different classes of molecules with activity against pathogenic microorganism, antimicrobial peptides (AMPs) have been proposed as a possible next generation of therapeutic agents [4–6]. Furthermore, AMPs can affect different pathogens or parasites ranging from bacteria, protozoa, and even virus.

AMPs consist of a group of short molecules, generally containing between 4 and 50 amino acids. More than 3000 AMPs have already been discovered in different living beings, from prokaryotic to unicellular eukaryotes, as well as multicellular organisms [7–9]. AMPs are rich in residues of arginine and/or lysine, which give them positive net charge

* Corresponding author.
** Corresponding author.
E-mail addresses: gvignoli@if.usp.br (G.S. Vignoli Muniz), mtlamy@usp.br (M.T. Lamy).

https://doi.org/10.1016/j.bbrep.2020.100827
Received 17 August 2020; Received in revised form 26 September 2020; Accepted 27 September 2020

when in physiologic pH. Moreover, due to the presence of hydrophobic and hydrophilic residues, AMPs present an amphiphilic character and many of these molecules interact strongly with amphiphilic aggregates and lipid bilayers [7]. Considering that AMPs are generally cationic, most of the studies emphasize their interaction with negative structures, particularly negative domains in lipid bilayers [10].

Nonetheless, the precise antibiotic mechanism of the AMPs is still a matter of debate [11–13]. For instance, it has been reported that some AMPs may act as destabilizing lipid bilayers, inducing membrane disruption. On the other hand, they could also act by either inducing changes in a cellular enzyme, and/or inhibiting nucleic acid synthesis [14,15]. As an example, the AMP coprisin (TCDVLSFEAKGIAVNHSACALHCIALRKKGGSCQNGVCVCRN) has the ability to cross the membrane of *Escherichia coli* without inducing membrane permeabilization, and once it is in the cytosol, this peptide induces the cell's death through apoptosis [16]. Moreover, some AMPs, such as Hecate (FALALKALKKALKKLKKALKKAL), and its analogue GA-Hecate, present a dual action: at low concentrations they induce apoptosis whereas at high concentration they provoke membrane disruption [15].

Like most drugs, AMPs can also cause damaging effects on mammalian cells. Hence, synthetic AMPs, based on the primary sequence of native AMPs, have been designed trying to magnify the cytotoxicity against pathogens and minimize any possible secondary effects on healthy cells [17].

The three peptides used in this work (Fig. 1) are based on the sequence of the native Hylin a1 (IFGAILPLALGALKNLIK) extracted from the skin secretion of the frog *Hypsiboas albopunctatus*. Hylin a1 (Hya1) presents a considerable hemolytic and a strong antimicrobial action [18]. The changes in the native sequence of Hya1 consist in the substitution of a leucine by a tryptophan (Trp) residue at the sixth position of the peptide chain (W^6Hya1), and a modification at the N-terminus group, with the insertion of an amino acid residue, either an aspartate residue (D^0W^6Hya1) or a lysine one (K^0W^6Hya1).

The changes in the natural sequence of the native Hya1 modulated the peptides toxicity against cultures of bacteria and fungus [19]. The introduction of a tryptophan residue (W^6Hya1), without modification of the peptide's net charge, resulted in an increase of activity against Gram-positive bacteria and fungus cultures, as well as a higher hemolytic action. Similarly, the addition of a negative charge (D^0W^6Hya1) enhanced the peptide antibiotic activity against Gram-positive bacteria, but a decrease against Gram-negative bacteria was observed [19]. The extra positive charge in the peptide chain (K^0W^6Hya1) expanded its antimicrobial spectrum, with activity against cultures of Gram-positive and Gram-negative bacteria and fungus, but an increase in its hemolytic action [19]. In addition, K^0W^6Hya1 also presents activity against planktonic and biofilm growth of oral bacteria [20], and it has been used in the control of bacterial diseases of citrus [21].

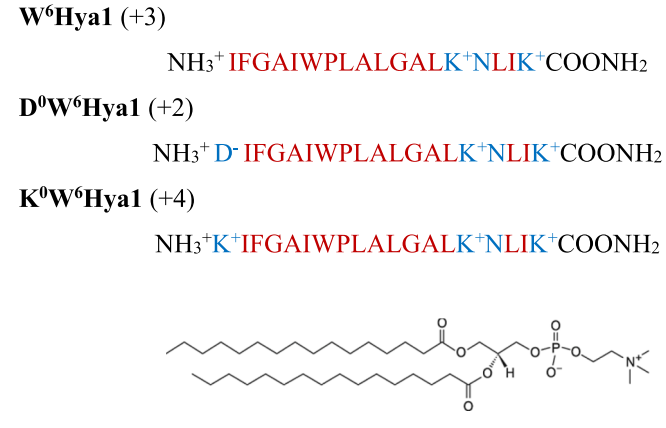

Fig. 1. Primary structures of W^6Hya1, D^0W^6Hya1 and K^0W^6Hya1, and the chemical structure of the lipid DPPC. Polar amino acid residues are drawn in blue and non-polar in red. The peptides net charges are indicated in parentheses. (For interpretation of the references to colour in this figure legend, the reader is referred to the Web version of this article.)

Furthermore, Hylin peptides are unstructured in water, whereas in the presence of zwitterionic micelles of LPC (dodecylphosphocholine) the peptides display an ordered secondary structure composed mostly by α-helix [19]. Previously, it has been shown that Hylin peptides interact with anionic amphiphilic aggregates [19,22]. The comparative interaction of K^0W^6Hya1 with zwitterionic and anionic membranes, mimicking mammalian and bacterial membranes, respectively, was investigated [23], showing that though the peptide interacts with DPPC (1,2-dipalmitoyl-*sn*-glycero-3-phosphocholine), its interaction with DPPG (1,2-dipalmitoyl-*sn*-glycero-3-phospho-(1′-*rac*-glycerol)) was much stronger.

The focus of the present work is a comparative study of the effects of the interaction of the three Hylin analogues, W^6Hya1 (+3), D^0W^6Hya1 (+2), and K^0W^6Hya1 (+4) with models of eukaryotic structures, namely DPPC, a zwitterionic lipid used here to mimic healthy mammalian membranes [24,25], and calf-thymus DNA (CT DNA), aiming at the design of healthier therapeutic agents. Different methodologies were applied, such as intrinsic Trp fluorescence, as the three peptides have a Trp residue, differential scanning calorimetry of DPPC membranes disturbed by the peptides, and the ability of the peptides to cause pore formation in PC membranes, through the measurement of the leakage of entrapped carboxyfluorescein (CF), a fluorescent dye, in PC large unilamellar vesicles. The interaction of the peptides with CT DNA was studied via both Trp fluorescence and by the competitive studies with CT DNA previously bound to ethidium bromide. Furthermore, the interaction of Hylin peptides with plasmid DNA was evaluated by electrophoresis experiments.

2. Materials & methods

2.1. Chemicals and reagents

1,2-dipalmitoyl-sn-glycero-3-phosphocholine (DPPC) and 1-palmitoyl-2-oleoyl-glycero-3-phosphocholine (POPC) were acquired from Avanti Polar Lipids. Calf-thymus DNA (CT DNA), 4-(2-hydroxyethyl)-1-piperazineethanesulfonic acid (HEPES), sephadex-G25 medium column, glucose, chloroform, ethylenediamine tetraacetic acid (EDTA), 3,8-Diamino-5-ethyl-6-phenylphenanthridinium bromide (EB), sodium hydroxide (NaOH), hydrochloric acid (HCl), and sodium chloride (NaCl) were purchased from Sigma Aldrich (St Louis, MO). The plasmid pOP3BP (pDNA) was kindly gifted from Marko Hyvönen (Dep. of Biochemistry, University of Cambridge). All solutions or dispersions were prepared with Milli-Q water or chloroform.

2.2. Peptide synthesis

The peptides were synthesized manually using the N-9-fluorenylmethoxycarbonyl (Fmoc) chemistry, purified, and characterized according to the experimental protocol, as described somewhere else [19]. The purity of the Hylin peptides was found to be higher than 98%, as attested by Reversed-phase high-performance liquid chromatography (RP-HPLC) (Fig. SM1).

2.3. Large unilamellar vesicle preparations

The desired amount of lipids was solubilized in chloroform. By using a flux of gaseous nitrogen, the solvent was evaporated and thus a thin film of lipids formed at the bottom of the glass tube. Then, the lipid film was kept under low pressure conditions for a minimum of 3 h. Aqueous dispersions were prepared by the addition of buffer (10 mmol L^{-1} HEPES, 3 mmol L^{-1} NaCl, pH 7.4) to the lipid film, followed by vortexing for 2 min at 50 °C. Finally, lipid dispersions were extruded through polycarbonate filters (mini-extruder by Avanti Polar Lipids, 19

mm membranes with 100 nm pores, 31 times) above the lipid gel−fluid transition temperature (≥50 °C), for the formation of large unilamellar vesicles (LUVs). All lipid dispersions used in this work were freshly prepared on the same day of the experiments. Through inorganic phosphate assay [26] we determined the lipid concentration before and after the extrusion process: the difference was smaller than 5%.

2.4. CT DNA stock solution

CT DNA was diluted into buffer (10 mmol L^{-1} HEPES, 3 mmol L^{-1} NaCl, pH 7.4), followed by intensive stirring for three days, and kept at 4 °C for no longer than a week.

The CT DNA concentration was determined by the UV absorbance at 260 nm after 1:20 dilution in water, using an extinction coefficient of the DNA per molar nucleotide concentration equals to 6600 L mol^{-1} cm^{-1} [27,28]. The stock solution of CT DNA gave a ratio of UV absorbance at 260 and 280 nm higher than 1.8, indicating that the CT DNA was sufficiently free of protein contamination.

2.5. Absorption spectroscopy

Optical absorption spectra were obtained with an UV–Vis spectrophotometer (VarianCary, Santa Clara, CA). Samples were placed in a quartz cuvette (0.4 × 1.0 cm), with the absorption optical pathway of 0.4 cm. The temperature was controlled with a Carry Peltier thermostat, and measurements were performed at 25 °C or 50 °C.

2.6. Fluorescence spectroscopy

Steady state fluorescence measurements were performed using a Fluorimeter (VarianCary, Santa Clara, CA) with slits for excitation and emission of 5 nm and a bandpass of 2 nm. Temperatures were controlled by a Carry Peltier thermostat. Fluorescence experiments were performed with 1 ml solutions of AMP (20 μmol L^{-1}) in buffer (HEPES 10 mmol L^{-1}, 3 mmol L^{-1} NaCl, pH 7.4), upon titration with DPPC vesicles or CT DNA. The membrane stock dispersion consisted of 10 mmol L^{-1} of extruded DPPC (100 nm), and CT DNA stock solution was approximately 3 mmol L^{-1}.

The experiments with membranes were conducted at DPPC gel (25 °C) and fluid phases (50 °C), with the excitation beam light at 280 nm. The experiments with CT DNA were performed at 25 °C. To avoid any absorption by DNA nucleobases, DNA experiments were performed with the excitation beam light at 295 nm. The fluorescence spectra were corrected by the appropriate dilution due to the addition of lipids or DNA. Moreover, the inner filter correction [29] was applied to all the fluorescent emission spectra by using Equation (1):

$$F_{corr}(\lambda) = F_{obs}(\lambda) 10^{(A_{exc}\, l + A_{ems}\, l')} \quad (1)$$

where F_{corr} (λ) and F_{obs} (λ) are the corrected and observed fluorescence intensity at a given λ, A_{exc} and A_{ems} are the absorbance per unit of pathway at the excitation and emission wavelengths, respectively. l and l′ are the optical pathways for excitation (0.2 cm), and for emission (0.5 cm), respectively. When necessary (Fig. SM2), the fluorescence spectra were transformed from wavelength to energy, and the intensity multiplied by λ^2. This procedure is necessary given that the emission spectrum is recorded with a constant wavelength bandpass, not energy [30,31].

2.7. Entrapment of carboxyfluorescein (CF) in LUVs and leakage assay

CF solutions were prepared in buffer pH 8.5. After CF solubilization, the sample pH was readjusted to 7.4 with HCl. Lipid films were hydrated with buffer (10 mmol L^{-1} HEPES, 3 mmol L^{-1} NaCl, 1 mmol L^{-1} EDTA, pH 7.4 solution) containing 50 mmol L^{-1} carboxyfluorescein (CF). The lipid dispersion (~6 mmol L^{-1}) was extruded, as previously described. In order to remove non-encapsulated CF, the lipid dispersion was eluted through a Sephadex-G25 medium column with 10 mmol L^{-1} HEPES, pH 7.4 with 1 $mmol^{-1}$ EDTA, 3 mmol L^{-1} NaCl, and 150 mmol L^{-1} glucose, the latter was added to the buffer to adjust the osmolarity inside and outside of the liposomes. Vesicles with encapsulated CF were collected in the void volume of the column. Lipid concentration was determined by inorganic phosphate assay [26].

Lipid dispersion (100 μmol L^{-1}) was placed in quartz cuvettes (1.0 × 1.0 cm, 2.0 mL) and the fluorescent emission measured with a Fluorescence Spectrometer (Varian Cary Eclipse, Santa Clara, CA), and the temperatures were controlled with a Carry Peltier thermostat. The CF release measurements were performed under constant stirring. CF encapsulating in LUVs was used as a model to evaluate the abilities of Hylin peptides to induce pore formation in zwitterionic bilayers. At 50 mmol L^{-1} the encapsulated CF is self-quenched, hence virtually non-fluorescent. Due to AMP or detergent action, CF might be released from the liposomes into the bulk, diluting CF and increasing the CF fluorescence intensity. CF emission was continuously recorded in time (one measurement per second), at 25 °C, λ_{exc} = 490 nm and λ_{em} = 512 nm. In all experiments, Hylin peptides (0.05 μmol L^{-1}) were added to lipid dispersion (100 μmol L^{-1}) at the 100th second and, at the end of the experiment, 2000th second, Triton X-100 (12 μL of 10% w/v) was added to promote complete CF leakage.

The percentage of CF leakage, (%) Leakage, was determined according to Equation (2):

$$(\%)\ Leakage(t) = 100 \times \frac{(I(t) - I_0)}{(I_{total} - I_0)} \quad (2)$$

where I(t) is the fluorescence intensity at time t, I_0 is the initial fluorescence, before peptide addition, and I_{total} is the maximum fluorescence obtained after the addition of Triton X-100. The kinetics were performed using zwitterionic liposomes of DPPC in the gel phase at 25 °C. As the experimental procedure with fluid DPPC (50 °C) was found to be quite unreliable [23], to mimic the fluid phase of the dipalmitoyl membranes, similarly prepared vesicles of POPC were used at 25 °C.

2.8. Differential scanning calorimetry (DSC)

DSC profiles were obtained with a microcalorimeter (Microcal VP-DSC, Northampton, MA). Samples were heated from 15 °C to 60 °C at a scan rate of 20 °C per hour. The sample cell (500 μL) was filled with a 3 mmol L^{-1} lipid dispersion with or without the addition of the desired AMP concentration. In this work, we will refer to the concentration of AMP as the percentage of the [AMP] with respect to the molar concentration of lipid (% [AMP] = 100 [AMP]/[L]), where [L] is the lipid concentration. We corrected the DSC traces taking into consideration the dilution due to the addition of the peptides. Baseline subtractions and peak integrals were performed using the MicroCal Origin software with the additional module for DSC data analysis provided by MicroCal.

2.9. Competitive studies with ethidium bromide (EB)

Ethidium bromide (EB) was solubilized in buffer (10 mmol L^{-1} HEPES, 3 mmol L^{-1} NaCl, pH 7.4) to make a stock solution (5 mmol L^{-1}), and submitted to ultrasound for 3 min to assure complete solubilization. The samples consist of 1 ml solution of EB (15 μmol L^{-1}) previously incubated with CT DNA (10 μmol L^{-1}) for 15 min to assure thermal equilibrium and the formation of the complex (EB-DNA; 15:10 in moles). Then, samples were placed in a quartz cuvette (0.4 × 1.0 cm, 1 ml). Finally, samples were titrated with Hylin peptides, and EB-CTDNA fluorescence spectra were measured. Experiments were performed with an excitation beam light at 545 nm.

2.10. DNA-binding assay

For Hylin analogues, W^6Hya1, D^0W^6Hya1, and K^0W^6Hya1, binding

reaction with plasmid DNA (plasmid pOP3BP, 4691 bp) was monitored using agarose gel electrophoresis. The nucleic acid binding efficiency was estimated by determining the degree of delayed mobility of the plasmid DNA (pDNA) bands, which is reflected in an up-shift of the DNA to higher molecular weight, indicating changes in the ratio of charge mass of the DNA-peptide complex [32]. Reactions containing 600 ng of pDNA and increasing amounts of each AMP in water for a final volume of 20 μL, were incubated at a constant temperature of 21 °C for 45 min. After incubation, 8 μl of each reaction was mixed with 2 μL of GelPilot DNA Loading Dye, 5x (QIAGEN), and submitted to electrophoresis on agarose gels (1% w/v), which contained 1X UniSafe Dye (UNISCIENCE), in TAE buffer (40 mmol L^{-1} Tris, 20 mmol L^{-1} acetic acid, and 1 mmol L^{-1} EDTA Sodium salt dihydrate), at 60 V during 90 min. Agarose gel electrophoresis was performed in a horizontal gel apparatus Mini-Sub Cell GT (BIORAD). The migration of pDNA was visualized after staining with the fluorescent intercalated UniSafe Dye under a UV illuminator. All experiments were repeated at least three times for reproducibility.

3. Results

3.1. Peptides interaction with zwitterionic membranes

Most of the bilayers composed of one saturated lipid species display two different thermal phases: a gel and a fluid phase. In the gel phase the lipid molecules are more organized and packed when compared to those in the fluid phase. In both phases, the lipid molecules are constrained to the two-dimensional plane of the membrane, but in the fluid phase the lipids are looser and can diffuse faster within the plane [33]. For DPPC membranes, the gel-fluid transition temperature is about 40 °C. The interaction of exogenous molecules with lipid membranes might be profoundly affected by the lipid phase [33]. Hence, we investigated the interaction of the three AMPs, W^6Hya1, D^0W^6Hya1, and K^0W^6Hya1, with DPPC membranes in their gel (25 °C) and fluid (50 °C) phases. That would somehow mimic both more packed and less packed lipid domains in biological membranes, respectively.

3.1.1. Fluorescence spectroscopy

The Hylin peptides studied herein are fluorescent due to the replacement of the leucine residue at the 6th position of the peptide chain by the aromatic tryptophan (Trp). To comparatively analyze Hylin peptides binding properties to eukaryotic-like membranes, we monitored the changes of AMP emission due to presence of DPPC LUVs.

Trp fluorescence spectrum is very sensitive to its environment [30], making it an excellent fluorescent probe to investigate changes in its vicinity. Accordingly, when a Trp residue moves to a more hydrophobic environment, its emission spectrum shifts to smaller wavelengths (higher energies), in comparison with the spectrum of the fluorophore in aqueous environment, as the dipolar relaxation decreases considerably [30]. Usually, parallel to that, there is an increase in the fluorescence intensity due to the reduction in non-radiative deactivation processes related with interactions with solvent molecules and/or a decrease of molecular mobility.

Let us compare the interaction of each peptide with zwitterionic LUVs of DPPC in the gel (25 °C) and fluid phases (50 °C). Fig. 2 exhibits the evolution of the AMPs intrinsic fluorescence emission spectra with increasing amounts of DPPC. It is evident that the three peptides bind to the zwitterionic membranes, at both gel (25 °C) and fluid (50 °C) bilayer phases, as the Trp fluorescence spectrum changes in the presence of DPPC. However, it is also evident that DPPC fluid membranes (Fig. 2, right column) induce stronger modifications on the Trp fluorescence spectra as compared to gel membranes (Fig. 2, left column).

To analyze and compare the changes caused by DPPC membranes on the Trp spectrum of the three peptides, the shifts on the position of the maximum emission of the three peptides in the presence of increasing amounts of lipids are shown in Fig. 3. For gel DPPC bilayers (Fig. 3a), the

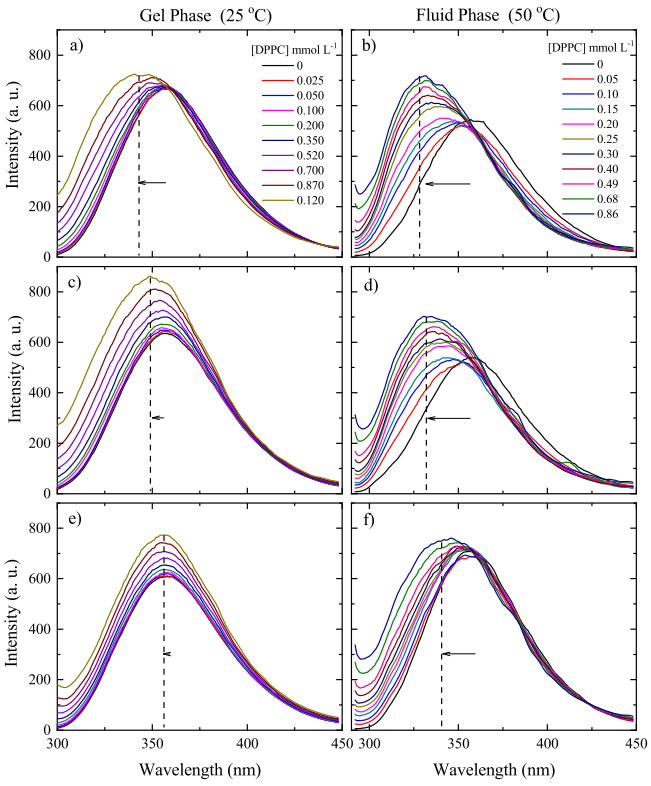

Fig. 2. Typical fluorescence spectra of W^6Hya1 (a, b), D^0W^6Hya1 (c, d), and K^0W^6Hya1 (e, f), obtained from titrating the peptide solution with gel (25 °C) (left column), and fluid (50 °C) (right column) vesicles of DPPC. λ_{exc} = 280 nm. AMPs concentration = 20 μmol L^{-1}. Dashed lines indicate the center (maximum) of the emission bands at the maximum lipid concentration used. The fluorescence intensities at these positions were used to calculate the apparent dissociation constant for each sample (Fig. 4 and Eq. (2)). Arrows indicate spectra shifts at the maximum lipid concentration.

Trp blue shifts are significantly smaller than those observed in the presence of fluid membranes (Fig. 3b). That indicates that either the peptides (or, at least, the Trp residue in the peptides) are deeper inside fluid DPPC bilayers as compared with gel membranes, and/or that the peptides exhibit a small partition into gel DPPC bilayers and stay mostly in the water medium.

For fluid DPPC membranes, the maximum lipid concentration used here is close to a lipid saturation concentration, where most of the peptides are bound to the membrane, as indicated by the flattening of the curves in Figs. 3b and 4b, for the highest DPPC concentrations used (around 1 mmol L^{-1}). Hence, it is possible to conclude that in fluid DPPC bilayers, Trp in the more charged peptide, K^0W^6Hya1 (net charge +4; ▼in Fig. 3b), is in a shallower position in the bilayer (smaller blue shift) as compared with Trp in the two other peptides, W^6Hya1 and D^0W^6Hya1 (net charges +3 (▱) and +2 (⊗), respectively, in Fig. 3b). Moreover, Trp in W^6Hya1 (▱) seems to be in a somewhat deeper position in the membrane (larger blue shift) than the residue in D^0W^6Hya1 (⊗).

For the three peptides, in both gel and fluid membranes, the blue shifts (Fig. 3) in the presence of the highest lipid concentrations used here are listed in Table 1. Higher lipid concentrations could not be used due to the significant light scattering yielded by them, making the inner filter corrections used here unreliable (see Materials and methods). Hence, even though the effect on the Trp fluorescence spectrum due to the peptides binding to gel DPPC is far from saturated, it follows the same trend observed for the peptides in fluid DPPC, with K^0W^6Hya1 (▼) displaying the least effect (Fig. 3a).

Apart from the blue shift caused by DPPC vesicles on the Trp spectrum, there is a clear increase in the spectrum intensity, mainly observed

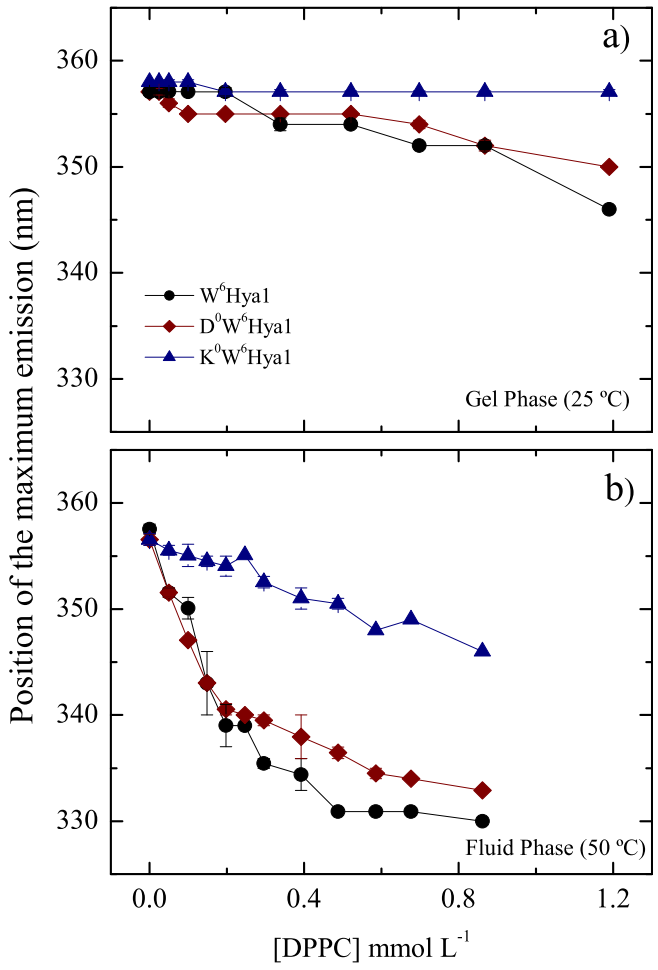

Fig. 3. Position of the maximum emission of W^6Hya1 (black circle), D^0W^6Hya1 (wine diamond), and K^0W^6Hya1 (navy triangle) as a function of DPPC concentration: (a) in the lipid gel phase (25 °C) and (b) in the fluid phase (50 °C). The AMPs concentration was 20 μmol L^{-1} λ_{exc} = 280 nm. Error bar indicates standard deviation of at least three experiments with different samples. If not shown, it was found to be smaller than the symbol. (For interpretation of the references to colour in this figure legend, the reader is referred to the web version of this article.)

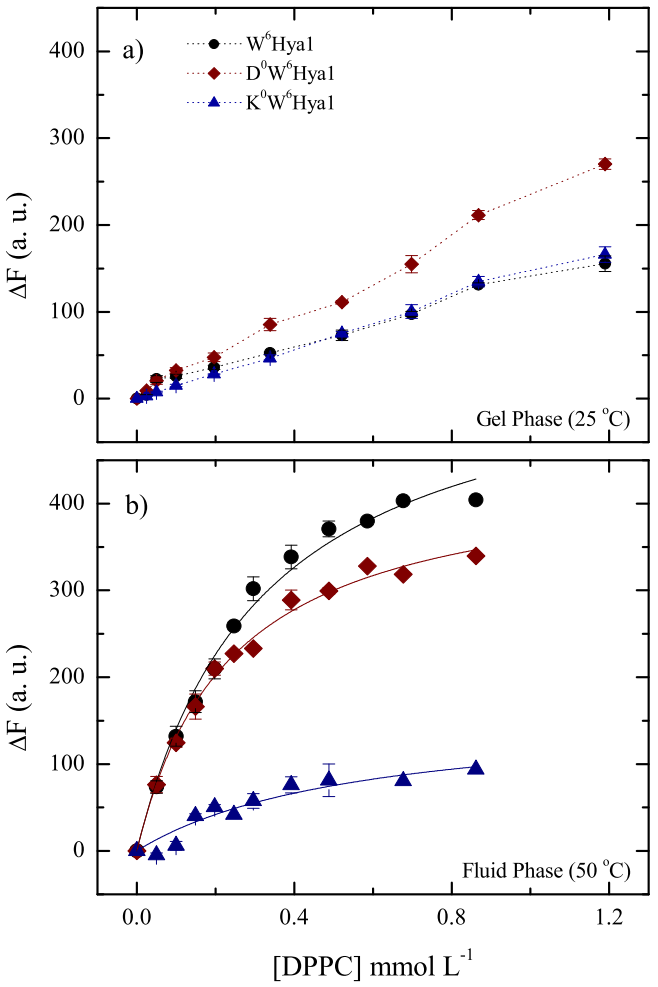

Fig. 4. Increase of the Trp fluorescence intensity (ΔF = F–F_0, F_0 being the fluorescence intensity in the absence of lipids), at the wavelength positions indicated in Fig. 2, of W^6Hya1 (black circle), D^0W^6Hya1 (wine diamond) and K^0W^6Hya1 (navy triangle), in the presence of DPPC vesicles in the (a) gel (25 °C) and (b) fluid (50 °C) lipid phases. λ_{exc} = 280 nm. The dotted lines are guides for eyes and full lines correspond to the fitting of the data with Eq. (3). AMPs concentration = 20 μmol L^{-1} λ_{exc} = 280 nm. Error bar indicates standard deviation of at least three experiments with different samples. If not shown, it was found to be smaller than the symbol. (For interpretation of the references to colour in this figure legend, the reader is referred to the web version of this article.)

in the presence of fluid DPPC membranes (Fig. 2, right column). This is also an indication that the Trp residue, in the peptides, is inserted into the membrane, in a microenvironment of lower polarity and/or more vibrational restriction. Hence, the variation of the fluorescence intensity (ΔF = F–F_0, F_0 being the fluorescence intensity in the absence of lipids) was plotted as a function of the lipid concentration, for the three peptides, in the membranes in both gel and fluid phases (Fig. 4). The fluorescence intensities were measured at the wavelength where the emission intensity is at its maximum in the presence of the highest lipid concentration used (see dashed lines in Fig. 2).

Similar to what was observed for the blue shift (Fig. 3a), the Trp fluorescence intensity variations in the presence of gel DPPC are not very intense (Fig. 4a), they do not saturate with the amount of lipids used here (around 1 mmol L^{-1}). That strongly suggests that at the DPPC gel phase most of the AMPs remain in the aqueous phase. Hence, it was not possible to address an apparent dissociation constant (K_d) for the peptides in the presence of gel DPPC vesicles.

However, the plots ΔF x [DPPC] obtained in the presence of fluid DPPC (Fig. 4b) could be well fitted with the conventional binding isotherm (Eq. (3), full lines in Fig. 4b):

Table 1
AMPs Trp blue-shifts due to the binding to DPPC vesicles at the highest lipid concentration used here, at gel (25 °C) and fluid (50 °C) lipid phases (data in Fig. 3). AMPs net charge are shown in parentheses.

AMP	$\Delta\lambda_{max}$ (nm) gel (25 °C)	$\Delta\lambda_{max}$ (nm) fluid (50 °C)
W^6Hya1 (+3)	(11.0 ± 0.3)	(27.5 ± 0.8)
D^0W^6Hya1 (+2)	(7.1 ± 0.2)	(24.6 ± 0.5)
K^0W^6Hya1 (+4)	(3.1 ± 0.8)	(11.5 ± 0.6)

$$\Delta F = F - F_0 = \frac{(F_\infty - F_0)[L]}{(K_d + [L])} \quad (3)$$

where F_∞ is the fluorescence intensity of the AMPs at lipid saturating concentration. The apparent dissociation constant (K_d) is the concentration of lipids which induces 50% of changes in the fluorescence intensity, under the experimental conditions employed. Here, we use K_d values to compare the affinities of the three AMPs to fluid DPPC

membranes, not for the actual measurement of a true partition constant. Hence, it is important to keep in mind that the apparent K_d calculated here does not take into consideration the increase of the membrane charge due to cationic binding peptides [34].

Table 2 displays K_d, ΔF_∞, and χ^2 values obtained through the best fitting processes. Note that the dissociation constant obtained for K^0W^6Hya1 is about two times higher than those obtained for the other two AMPs. However, the nonlinear least squares fit for K^0W^6Hya1 yielded a χ^2 value equal to 0.90, indicating that this K_d value has a high associated error. This occurs due to the low affinity of this peptide to DPPC membranes, rendering the determination of F_∞ rather inaccurate. It is interesting to observe that K_d values follow the crescent order D^0W^6Hya1 (+2) < W^6Hya1 (+3) < K^0W^6Hya1 (+4). It is important to keep in mind that a higher K_d value reflects a lower affinity to DPPC membrane. Therefore, the net charge dependence is clearly indicating that the increase of a positive charge at the N-terminus of the peptide hampers the AMP association to zwitterionic membranes.

To use the variations on the Trp fluorescence intensity to discuss the penetration of the peptides into the lipid bilayer, we should look at the values of ΔF_∞ (Eq. (3) and Table 2), as, theoretically, this is the value obtained when all peptides are bound to the vesicles. In accord with the blue shift (Fig. 3 and Table 1), they indicate that Trp in W^6Hya1, is somehow deeper in the membrane ($\Delta F_\infty = 59$) than the residue in the other two peptides. Moreover, the significant lower ΔF_∞ value obtained for the more cationic peptide (K^0W^6Hya1) ($\Delta F_\infty = 17$) strongly indicates that the double positive charge at its N-terminal keeps this peptide less deep in the membrane as compared with D^0W^6Hya1 ($\Delta F_\infty = 44$).

Though there is no theoretical argument for associating a binding isotherm, like Eq. (3), with the shift of the maximum of the emission band, it was interesting to find that the plots of ΔF x [DPPC] (Fig. 4, and Table 2) and ΔE x [DPPC] behave similarly, as shown in Fig. SM2 and Table SM1, displaying the same trend. ΔE is $E - E_0$, where E is the energy of the emission band corresponding to the maximum position of the band, and E_0 is the value in the absence of lipids.

3.1.2. *Differential scanning calorimetry (DSC)*

Saturated lipid bilayers often display a very narrow peak of heat capacity which is characteristic of a cooperative process, being very dependent on lipid-lipid interaction. As the presence of an exogenous molecule may interfere with the phase transition process, DSC thermograms can provide important information about the interaction of exogenous molecules with lipid systems [35].

In particular, multilamellar DPPC membranes (non-extruded) display a very characteristic pre-transition peak centered at about 33 °C and a thin main transition peak around 40 °C. Whereas, 100 nm extruded lipid dispersions of DPPC (Large Unilamellar Vesicles, LUVs) exhibit a subtle pre-transition peak and a less cooperative main transition peak about the same temperatures observed for multilamellar DPPC dispersions [23,33].

Fig. 5 displays DSC profiles of DPPC LUVs in the absence and presence of increasing amounts of W^6Hya1 (Fig. 5a), D^0W^6Hya1 (Fig. 5b), and K^0W^6Hya1 (Fig. 5c). Increasing amounts of the three peptides cause similar effects on the DPPC thermogram, and similar to that reported before for K^0W^6Hya1 [23]. The broadening of the DPPC bilayer transition observed in the presence of the three peptides suggest a homogeneous perturbation of the lipids due to peptide binding, decreasing the cooperativity of the gel-fluid transition. That is, there is no indication of the coexistence of peptide-bound and peptide-free regions (bulk lipid) in the bilayer, as observed with K^0W^6Hya1 in the presence of anionic DPPG membranes [23]. The enthalpy of the main transition remains roughly the same for all samples studied, $\Delta H \approx 8$ kcal mol^{-1}, in accord with previous studies with pure DPPC [36]. Though this was not investigated

Table 2
Apparent dissociation constants of the three AMPs for fluid (50 °C) DPPC membranes, obtained from steady-state fluorescence spectroscopy (data in Fig. 4). AMPs net charge are shown in parentheses.

AMP	K_d [× 10^{-4} mol L^{-1}]	ΔF_∞[× 10 a. u.]	χ^2
W^6Hya1 (+3)	(3.2 ± 0.3)	(59 ± 2)	0.99
D^0W^6Hya1 (+2)	(2.4 ± 0.2)	(44 ± 1)	0.99
K^0W^6Hya1 (+4)	(6 ± 3)	(17 ± 4)	0.90

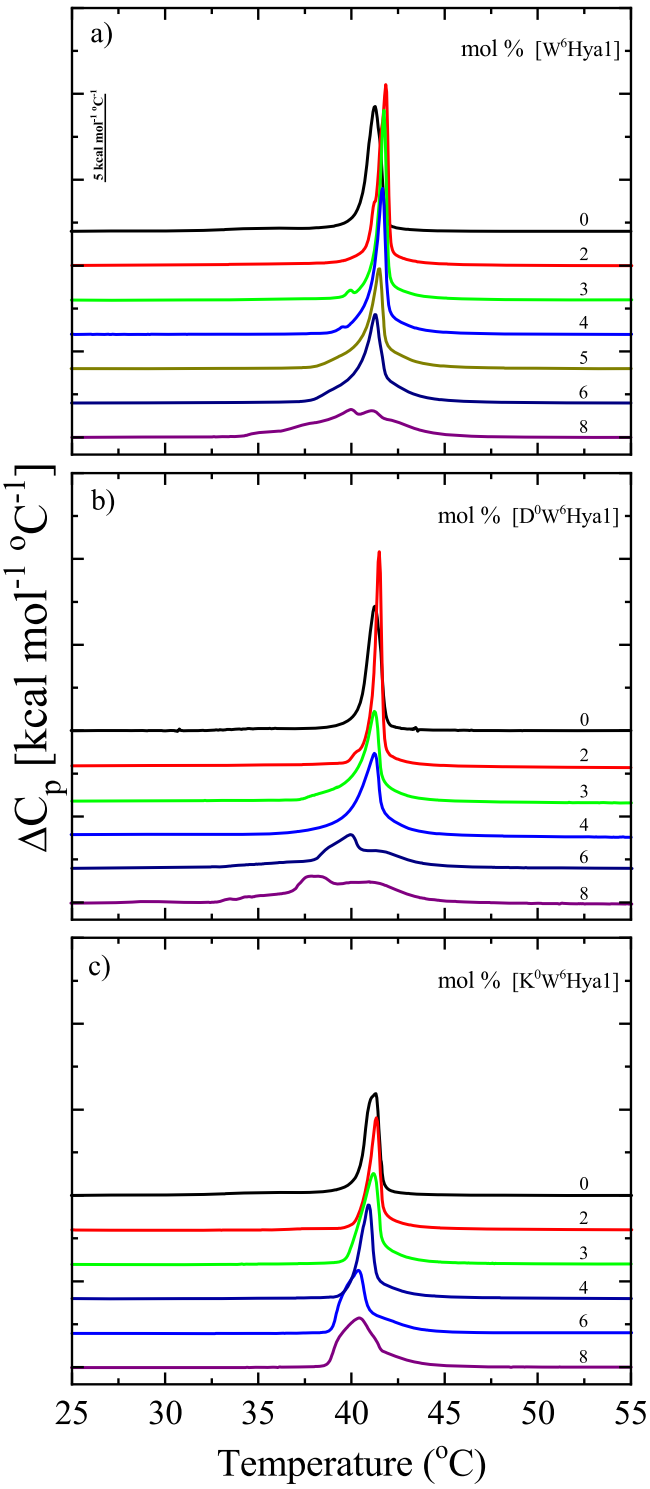

Fig. 5. DSC thermograms of 100 nm extruded lipid dispersions composed of 3 mmol L^{-1} DPPC with increasing peptide–lipid molar ratio, from 2% to 8% of (a) W^6Hya1 or (b) D^0W^6Hya1 and (c) K^0W^6Hya1. Scans were obtained using a scan rate of +20 °C/h, and they are shifted for clarity. Duplicated samples showed similar results.

in the present work, it is interesting to note that the lowest peptide concentration used here (2 mol%) causes a slightly narrowing of the thermal transition (Fig. 5).

All thermograms were found to be not only reproducible, in a second scan, but also reversible (Fig. SM3), supporting the assumption that the three peptides cause a homogeneous effect on the bilayer. Furthermore, DSC thermograms seem to be in agreement with the fluorescence findings which shows that the most cationic peptide displays a lower affinity and a shallower interaction with DPPC membranes (Tables 1 and 2). Namely, at 8 mol%, K^0W^6Hya1 is less effective in disturbing DPPC thermograms, as it is still possible to observe a well resolved thermal peak, whereas for the two other peptides, at this same concentration, a very broad band is observed.

3.1.3. Carboxyfluorescein (CF) leakage assay

It was previously shown that the cationic peptide K^0W^6Hya1 could not only disturb anionic membranes, but also causes a significant leakage of carboxyfluorescein (CF) through zwitterionic PC membranes [23], at rather low peptide/lipid relative concentration. Hence, we compare the effect of the three peptides studied here, with different net charges, on the leakage of CF through PC membranes. Similar to previous results [23], Fig. 6 shows that a very small peptide/lipid relative concentration (0.05 mol%) is enough to cause a significant leakage in fluid POPC membranes, and has almost no effect on gel DPPC bilayers, both at 25 °C. Very interesting to note that the more cationic peptide, K^0W^6Hya1, is the one that causes the major leaking at the end of the process, after 2000 s, in fluid PC vesicles. The spontaneous CF release, in the absence of peptides, was found negligible (less than 2% in 2000 s), as the control consists of liposomes containing CF in the absence of peptides. As found for many CF-leakage experiments [37–39] the kinects were well fitted by two exponentials, indicating two kinect processes, with different decay times (Fig. SM4). Indeed, this finding is in agreement with existing data for the interaction of K^0W^6Hya1 with PC vesicles [23]. Important to have in mind that at the concentrations used here the peptides do not significantly change the size of the vesicles, as attested by dynamic lighting scattering experiments (not shown).

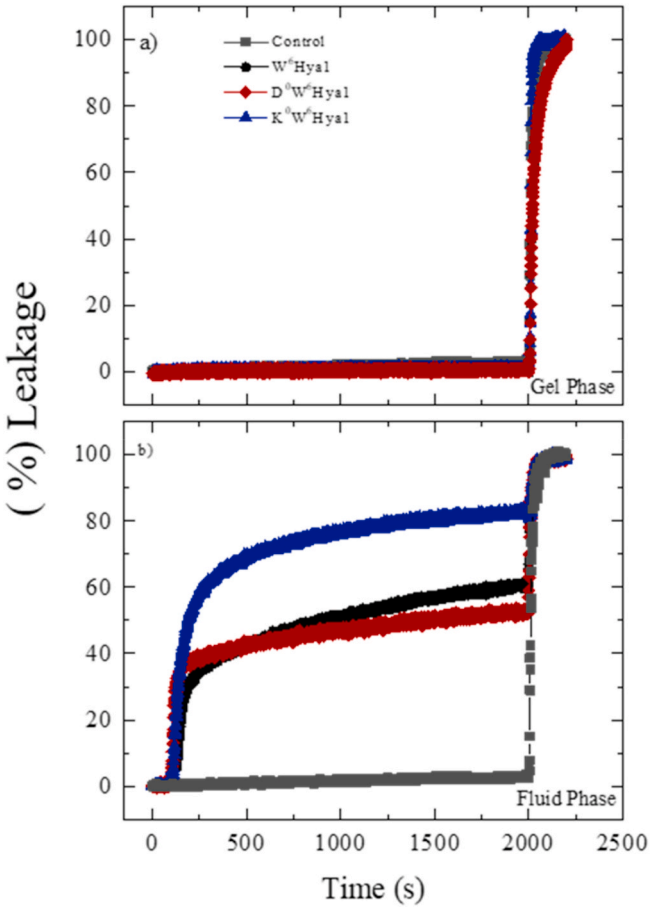

Fig. 6. Typical kinetics of CF leakage through LUVs composed of gel membranes of DPPC (a), and fluid membranes of POPC (b), at 25 °C, in the presence of 0.05 μmol L^{-1} of W^6Hya1 (black circle), D^0W^6Hya1 (wine diamond) and K^0W^6Hya1 (navy triangle). Lipid concentration used was 100 μmol L^{-1}. The control (gray square) consists of pure PC LUVs. (For interpretation of the references to colour in this figure legend, the reader is referred to the web version of this article.)

3.2. Hylin peptides interaction with DNA

Since Hylin peptides form pores in zwitterionic lipid bilayers, we can presume that they will invade cell cytosol. Therefore, we found important to inquire about Hylin peptides interaction with structures present in the cellular cytosol, such as nucleic acids. Indeed, several peptides show nucleic acid binding abilities [40–42]. Due to electrostatic interaction, it was expected that cationic AMPs would display DNA-binding activity.

3.2.1. Trp fluorescence spectroscopy with CT DNA

We comparatively evaluated the interaction of Hylin peptides with CT DNA, through intrinsic AMPs fluorescence spectroscopy. Fig. 7 displays the normalized spectra of Hylin peptides, W^6Hya1 (Fig. 7a), D^0W^6Hya1 (Fig. 7b), K^0W^6Hya1 (Fig. 7c), with increasing amounts of CT DNA. Note that in the presence of CT DNA, the peptides exhibit a significant blue shift: Fig. 7d is the plot of the position of the Trp maximum emission in each peptide versus CT DNA concentration (in pair base molar concentration). Upon CT DNA titration, the peptides absorption spectra display significant light scattering (Fig. SM5), mainly for CT DNA concentrations above 40 μmol L^{-1}, rendering quite inaccurate the values of the measured fluorescence intensities, even after the corrections used here (see Material and methods). Hence it was not possible to calculate an apparent binding constant for the peptides with CT DNA, as shown in Eq. (3).

The maximum blue shifts ($\Delta\lambda_{max}$) observed at the highest CT DNA concentration used here (80 μmol L^{-1}) for the Hylin peptides are listed in Table 3. We observe significant blue shifts due to the presence of CT DNA: W^6Hya1 (+3) and K^0W^6Hya1 (+4) display a maximum blue shift of about 17 nm. In contrast, the interaction of the peptide D^0W^6Hya1 (+2) with CT DNA shifts the emission peak 10 nm only. The observed blue shifts indicate that the polarity in the vicinity of the Trp residues has changed, this could be correlated with DNA binding and/or conformational changes in the Hylin peptides.

3.2.2. Competitive CT DNA-binding between ethidium bromide and hylin peptides

The interaction of exogenous molecules and DNA can be driven by covalent and non-covalent interactions, the later are notably divided in two binding modes: intercalative and groove. In the intercalative binding mode, the molecules allocate themselves into DNA double helix adjacent to the nucleobases, whereas in the groove binding mode the molecules interact with the negative sugar-phosphate DNA backbone, mediated by electrostatic and hydrogen bond interactions. Usually small molecules can bind to DNA by more than only one mode [43,44].

The observed Trp blue shifts for Hylins in the presence of DNA show that these peptides interact with DNA. To verify if Hylin peptides bind to DNA via the intercalative mode, we evaluated the ability of the peptides to displace ethidium bromide (EB), previously bound to CT DNA. EB is a dye that intercalates into DNA double helix. It does not exhibit a significant fluorescence when in aqueous solution. In contrast, when intercalated into DNA double helix, EB emission increases considerably [29]. If Hylin peptides intercalate into DNA, they would compete with EB for the same hydrophobic site in the DNA double helix, eventually

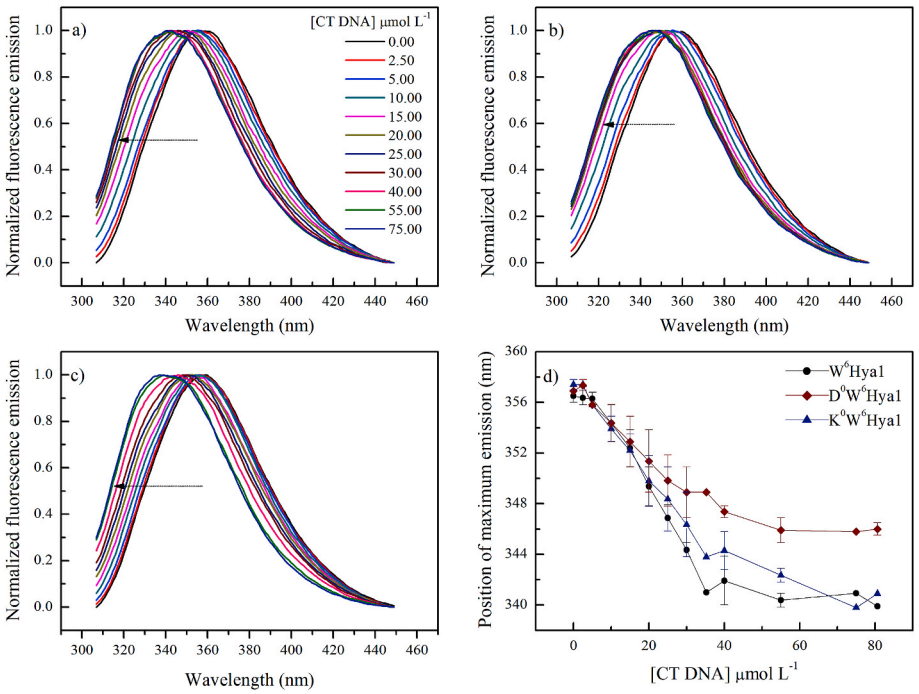

Fig. 7. Typical normalized fluorescence spectra of (a) W^6Hya1, (b) D^0W^6Hya1, (c) K^0W^6Hya1 with increasing CT DNA concentrations. The arrows are guides for eyes, indicating the Trp blue shift. (d) Position of the maximum emission of W^6Hya1 (black circle), D^0W^6Hya1 (wine diamond), and K^0W^6Hya1 (navy triangle) as a function of CT DNA concentration. λ_{exc} = 295 nm. Error bar in (d) indicates standard deviation of at least three experiments with different samples. If not shown, it was found to be smaller than the symbol. (For interpretation of the references to colour in this figure legend, the reader is referred to the Web version of this article.)

Table 3
AMPs Trp blue-shifts due to the presence of CT DNA at the highest lipid concentration used here. (data in Fig. 7). The AMPs net charges are shown in parentheses.

AMP	$\Delta\lambda_{max}$ (nm)
W^6Hya1 (+3)	(16.8 ± 0.2)
D^0W^6Hya1 (+2)	(10.9 ± 0.5)
K^0W^6Hya1 (+4)	(16.5 ± 0.4)

displacing EB to the aqueous environment, hence leading to a decrease of EB intensity emission.

Fig. 8 shows the EB-DNA fluorescence spectra with increasing amounts of Hylin peptides: W^6Hya1 (Fig. 8a), D^0W^6Hya1 (Fig. 8b) and K^0W^6Hya1 (Fig. 8c). It evinces that the Hylin peptides decrease the emission intensity of EB-DNA complex (Fig. 8), indicating that Hylin peptides are binding the DNA by the intercalative mode, thus dislocating EB molecules. Hence, the Stern-Volmer plot (Fig. 8d) and Eq. (4), seems to be appropriated to quantify and compare Hylin peptides abilities to

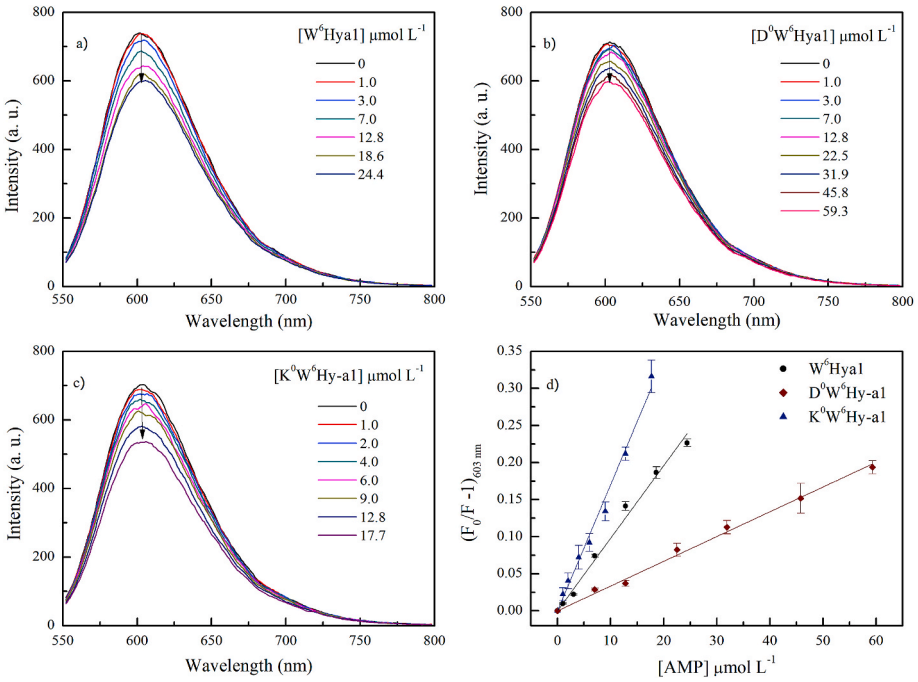

Fig. 8. – Typical Fluorescence spectra of the complex EB-DNA with increasing amounts of: (a) W^6Hya1, (b) D^0W^6Hya1, (c) K^0W^6Hya1. (d) Stern-Volmer plots (Eq. (4)) versus AMPs concentration. λ_{exc} = 545 nm, λ_{ems} = 603 nm. The arrows are guide for the eyes only, indicating increase amounts of AMPs. Error bar in (d) indicates standard deviation of at least three experiments with different samples. If not shown, it was found to be smaller than the symbol.

intercalate into DNA double helix. It is important to note that the Stern-Volmer equation will be used here not to monitor fluorescence quenching, as it is usually applied, but to monitor the decrease in the EB fluorescence due to the decrease in the concentration of EB-DNA complex.

$$F_0/F - 1 = K_{SV}[AMP] \quad (4)$$

Where F_0 and F, are the fluorescence intensities at the maximum emission of the complex EB-DNA (at 603 nm) in the absence of Hylin peptides and with increasing amounts of them, respectively, and K_{SV} is the Stern-Volmer constant.

As mentioned above, we used the Stern-Volmer constant, Table 4, only to compare the ability of the Hylin peptides to dislocate EB from the DNA to the aqueous environment, hence associated with the peptide ability to intercalate into DNA: a higher K_{sv} value indicates a higher intercalative binding mode.

3.2.3. Agarose gel electrophoresis: binding experiments with plasmid DNA (pDNA)

We further investigated Hylin – DNA binding abilities through electrophoretic experiments, which can provide information about interactions of DNA with exogenous molecules such as AMPs. The technique consists of observing DNA pattern migration in agarose gel while it is submitted to a constant electric field. The nucleic acid binding efficiency can be estimated by determining the degree of delayed mobility of a DNA band reflecting in an upshift of the DNA to higher molecular weight.

Fig. 9 displays the electrophoresis mobility of pDNA in agarose gel in the absence and presence of increasing amounts of each of the three AMPs. The results show that AMPs interact with pDNA retarding its migration in a concentration-dependent manner. The greater the relative concentration of peptide the greater the DNA upshift. Corroborating our previous results from assays of Trp fluorescence spectroscopy with CT DNA (Table 3) and binding competition between ethidium bromide and Hylin peptides (Table 4), W^6Hya1 (+3) and K^0W^6Hya1 (+4) show similar retarding in the DNA migration at lower concentrations (see AMP/pDNA weight ratio 2.1 in Fig. 9), and the less cationic peptide D^0W^6Hya1 only induces a marginal effect on DNA migration at 2.1 (peptide:DNA).

At AMP/pDNA weight ratio of 0.6, we did not observe any significant changes in the DNA migration pattern of the three samples when compared to the control, and at the highest peptide concentration (weight ratio of 16.7) there was no DNA migration: pDNAs at the highest AMP/pDNA concentration remains within the well.

4. Discussion

Given the presence of many hydrophobic amino acid residues (Fig. 1), it was expected that Hylin peptides would interact with zwitterionic amphiphilic aggregates, as attested by the present experiments, and previous data [19,22]. As reported before for K^0W^6Hya1 [23], the three peptides studied here seem to laterally diffuse in DPPC membranes, inducing a progressive broadening of DPPC thermograms as the peptide concentration increases. Considering that there is no indication of the coexistence of peptide-bound and peptide-free regions in the bilayer, as observed with K^0W^6Hya1 in the presence of anionic DPPG membranes [23], it is highly likely that the peptides are laterally diffusing in the membrane, causing a time-average or space-average effect in the bilayer DSC profile (Fig. 5). The peptide lateral diffusion seems to happen in the gel and fluid phases of the membrane, as DSC profiles are fairly reversible (Fig. SM3).

For fluid membranes, we determined that the apparent affinity for DPPC membrane follows the decreasing order: D^0W^6Hya1 (+2) > W^6Hya1 (+3) > K^0W^6Hya1 (+4) (Table 2). This finding follows the same decrescent order of hydrophobicity determined by Ref. [19] for these peptides. It indicates that the net charge of the peptide modulates its hydrophobicity, hence, its affinity for zwitterionic membranes: the membrane apparent affinity decreases as the peptide net charge increases.

However, the depth of the peptide penetration into fluid PC bilayer, at least that of the Trp residue in the peptide, follows a somewhat different order: W^6Hya1 (+3) > D^0W^6Hya1 (+2) » K^0W^6Hya1 (+4). That is given by the values of $\Delta\lambda_{max}$ in Table 1, and those of ΔF_∞ in Table 2. It shows that the extra charge at the N-terminal (D^0) somehow prevents a deeper penetration of D^0W^6Hya1 (+2) into the bilayer, though it gives it a higher apparent affinity for PC membranes, as compared with W^6Hya1 (+3).

Therefore, our data show that the presence of an extra positive charge at the N-terminal of the peptide (K^0W^6Hya1), as compared with an extra negative charge (D^0W^6Hya1), drastically decreases both the binding constant and the penetration depth of the peptide into zwitterionic membranes. That is interesting, as it does not agree with previous results with molecular dynamics, which indicated that both D^0W^6Hya1 and K^0W^6Hya1 interacted similarly with zwitterionic lipid structures (micelles of dodecylphosphocholine [22]). It is important to point out that although micelles present similarities with membranes, since they are formed by amphipathic molecules, micelles are much more disordered structures.

The large blue shifts found for the Trp in W^6Hya1 and D^0W^6Hya1 in fluid PC bilayers, around 25 nm, are similar to those found for Trp deep in the bilayer in transmembrane peptides [45–48]. Hence, these two peptides, though diffusing in the membrane, are deeply immersed into the bilayer, either as transmembrane peptides or at the membrane surface.

The most cationic peptide K^0W^6Hya1 (+4) is the one that displays the lowest affinity for fluid PC membranes, and the one that binds at the shallowest bilayer position (Trp location). Accordingly, at 8 mol%, it is the one that less disturb the DPPC gel-fluid transition (Fig. 5c). Therefore, it was noteworthy that this peptide was the most efficient in causing CF leakage through fluid PC vesicles after around 30 min (Fig. 6). Though further investigation is certainly necessary, it is interesting to compare this finding with previous results that showed that although K^0W^6Hya1 binds deeper and stronger in anionic than in zwitterionic membranes, its efficiency in causing CF leakage was found to be much higher in fluid PC than PG vesicles [23]. The authors suggested that the peptide would be located at the surface of zwitterionic vesicles, laterally diffusing on it, triggering the opening of transient membrane polar pores due to the overlapping of irregular lipid packing zones, a mechanism proposed by Ref. [49]. In contrast, in anionic bilayers, K^0W^6Hya1 would be deeply embedded and strongly attached to the bilayer.

Accordingly, we could speculate that due to K^0W^6Hya1 lower affinity for PC vesicles and its shallower position on the membrane, as compared with W^6Hya1 and D^0W^6Hya1, K^0W^6Hya1 would be available to interact with more vesicles in a certain interval of time than the other two peptides, causing transient disruptions on the membrane. Hence, this could possibly explain the higher % of CF release observed after the 2000^{th} second for this peptide as compared with the other peptides. In the same trend, the AMPs Mac1 and aurein present greater affinity to anionic bilayers but they are more efficient to induce CF leakage in zwitterionic vesicles than in anionic [50].

Concerning the interaction of Hylin peptides with CT DNA, the blue

Table 4
Stern-Volmer constants of EB-DNA with Hylin peptides, from Fig. 8d and Eq. (4).

AMP	K_{SV} [$\times 10^4$ L mol^{-1}]
W^6Hya1 (+3)	(0.97 ± 0.03)
D^0W^6Hya1 (+2)	(0.33 ± 0.06)
K^0W^6Hya1 (+4)	(1.7 ± 0.4)

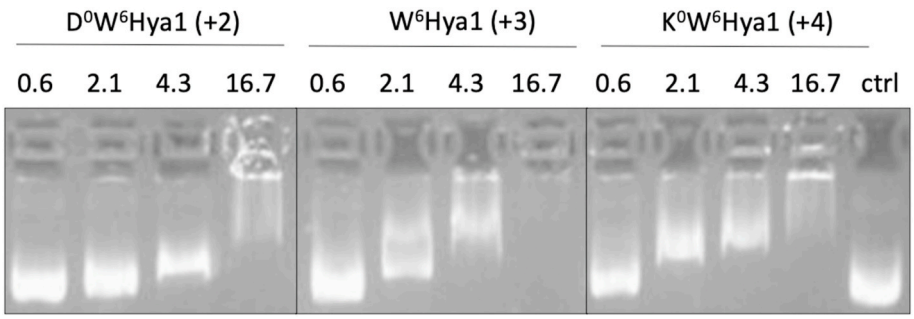

Fig. 9. Inhibition of the plasmid DNA (pOP3BP) mobility in agarose (1% w/v) gel electrophoresis upon addition of increased amount of Hylin peptides. Different amounts of peptides were incubated with 600 ng of pOP3BP plasmid DNA at room temperature for 60 min, and the reaction mixtures were applied into the gel. The relative AMP/pDNA weight ratio are indicated in the lane references and the control consists of plasmid DNA only. The results shown are representative of three experiments.

shifts observed are considerably large and follow a trend similar to those observed for the experiments with EB-peptide competition binding to DNA (see Tables 3 and 4), suggesting that the hydrophobic moiety of the peptides is imbedded into the DNA double helix. Indeed, Hylin peptides have considerable DNA intercalative binding abilities, as attested by the Stern-Volmer (K_{SV}) values in Table 4. As a comparison, synthetic antibiotics from the fluoroquinolone family are also known to intercalate into DNA. Stern-Volmer constants determined by the decrease of the EB-CT DNA fluorescence due to the presence of several fluoroquinolones are in the same order of magnitude, 10^4 L mol^{-1} [51]. The AMP AN5-1 (YSKSLPLSVLNP) also shows ability to decrease EB-CT DNA fluorescence with a K_{SV} of the same order mentioned above [52]. However, other drugs present a K_{SV} of two orders of magnitude higher than those observed by us [53]. Intercalant molecules can exhibit a cytotoxicity, as they can promote breaks and/or prevent the proper functions of the enzymatic cellular machinery, thus interfering in the processes of transcription and/or DNA replication, which can result in cell apoptosis [44,54].

Given the electrostatic interaction between the DNA anionic phosphate groups and the cationic peptides, a groove binding mode between Hylin peptides and DNA might also exist. It is quite common that a charged molecule interacts with DNA through both intercalative and groove binding modes [43,55]. Nonetheless, some molecules only interact via one binding mode, either intercalative or groove binding. For example, the synthetic lipophilic peptides, OA-C1b and LA-C1b, based on the sequence of the highly cationic chensinin-1b (+9) interact with CT DNA presenting a Trp blue shift of 9 nm, but the data indicate that these peptides interact mostly with the anionic phosphate group, since no evidence was found of intercalative binding mode [56]. Similarly, the synthetic aromatic tripeptide Phe-Phe-Phe (FFF), with a null net charge, interacts with CT-DNA but also only exhibits DNA groove binding activity, since it does not displace EB from the DNA double helix [57].

Electrophoresis experiments with the peptides and pDNA follow the same trend as that observed for the Trp blue shifts and K_{SV} values obtained for the peptides interaction with CT-DNA. Namely, W^6Hya1 and K^0W^6Hya1 display nearly the same effect on the pDNA migration pattern, whereas D^0W^6Hya1 is less effective in inducing changes in the pDNA migration (Fig. 9). Similarly, the interaction of D^0W^6Hya1 with CT-DNA yields the smallest values of Trp blue shift and K_{sv} (Tables 3 and 4).

Several factors drive the interaction of AMP with plasmid DNA. For example, the cationic AMP Magainin 2 (+3), which consists in 23 amino acid residues, only prevents total retardation in DNA electrophoresis migration with peptide/pDNA weight higher than 100 [58], whereas Indolicidin an AMP with 13 amino acid residues and a net charge of (+4) is able to promote complete retardation in pDNA electrophoresis experiments with a peptide/pDNA ratio of only 0.6 [59]. Taken this examples as lower and upper limit, we can conclude that the Hylin peptides studied here have a considerable DNA-binding activity since they can induce complete DNA retardation at the relative AMP/pDNA weight ratio of 16.7.

5. Conclusion

This work shows that the net positive charge of AMPs can determine its effective dissociation constant to zwitterionic membranes. From the intrinsic Trp fluorescence experiments, we showed that all three peptides bind zwitterionic bilayers, presenting a higher affinity to fluid than gel membranes. The affinity for fluid DPPC bilayers follows the decrescent order D^0W^6Hya1 (+2) > W^6Hya1 (+3) » K^0W^6Hya1 (+4). Fluorescence data also indicate that the Trp residue in the more positively charged peptide, K^0W^6Hya1, is less deep in the bilayer than the residue in the other two peptides. This finding is supported by DSC data, which shows that both D^0W^6Hya1 and W^6Hya1 disturbs DPPC gel-fluid transition slightly more effective than K^0W^6Hya1. It is important to note that the extra negative charge at the peptide N-terminal keeps the Trp residue in D^0W^6Hya1 in a shallower position in the zwitterionic membrane as compared with the residue in W^6Hya1.

The peptide, K^0W^6Hya1, displays the lowest affinity for PC fluid membranes and is located at the most superficial position in the bilayer. This peptide also happens to be the most efficient in causing pore formation in the membrane, as attested by CF leakage assays. As DSC data indicate that the three peptides laterally diffuse in PC membranes, it would be very interesting to find out why K^0W^6Hya1 can induce a higher leakage in zwitterionic vesicles. It should be important to find out if this is a particular result for these three peptides or if it is part of a more general trend.

The three Hylin a1 analogues studied here present DNA-binding activity. They exhibit a large Trp blue shift in the presence of CT DNA, and intercalate into DNA double helix, since they displace EB from the DNA pocket. W^6Hya1 (+3) and K^0W^6Hya1 (+4) are more efficient in binding DNA than the less cationic peptide D^0W^6Hya1 (+2), as attested by Trp fluorescence blue shifts, electrophoresis experiments, and EB competitive studies. These peptides display a considerable DNA binding activity since they could stop pDNA electrophoretic migration at AMP/pDNA weight ratio of 16.7. Hence, our findings suggest that the antibiotic action of Hylin peptides may also involve DNA-binding in addition to membrane interaction, albeit further investigations are necessary to better comprehend the Hylin peptides mechanism of action in cells.

The results shown here demonstrates that the peptide net charge is relevant and can modulate its interaction with eukaryotic structures such as zwitterionic bilayers and DNA. These findings could help the design of new therapeutic agents, balancing its antimicrobial and toxic effects.

Author contribution

Gabriel S. Vignoli Muniz: Investigation, data analysis, and writing-original draft preparation. **Lilia I. De la Torre:** Investigation, DNA electrophoresis experiments. **Evandro L. Duarte:** Investigation, data analysis and conceptualization **Esteban N. Lorenzón** and **Eduardo M. Cilli**: Peptide synthesis. **Andrea Balan**: DNA electrophoresis experiments. **M. Teresa Lamy**: Supervision, Writing-Reviewing and Editing.

Declaration of competing interest

There is no conflict of interest among authors.

Acknowledgment

This work was supported by the Brazilian agencies CNPq, FAPESP (2017/25930–1). E.M.C., A.B. and M.T.L. are recipient of CNPq research fellowships. G.S.V.M., E.L.D. and M.T.L. are part of the National Institute of Science and Technology Complex Fluids (INCT-FCx), financed by CNPq (465259/2014–6 and 405637/2017–1) and FAPESP (2014/50983–3 and 2018/20162–9). L. I. D. l. T. has scholarship from the Colombian COLCIENCIAS agency.

Appendix A. Supplementary data

Supplementary data to this article can be found online at https://doi.org/10.1016/j.bbrep.2020.100827.

Transparency document

Transparency document related to this article can be found online at https://doi.org/10.1016/j.bbrep.2020.100827.

References

[1] G.L. French, The continuing crisis in antibiotic resistance, Int. J. Antimicrob. Agents 36 (2010), https://doi.org/10.1016/S0924-8579(10)70003-0. S3–S7.
[2] G.M. Rossolini, F. Arena, P. Pecile, S. Pollini, Update on the antibiotic resistance crisis, Curr. Opin. Pharmacol. 18 (2014) 56–60, https://doi.org/10.1016/j.coph.2014.09.006.
[3] R. Wu, L. Wang, H.-C.D. Kuo, A. Shannar, R. Peter, P.J. Chou, S. Li, R. Hudlikar, X. Liu, Z. Liu, G.J. Poiani, L. Amorosa, L. Brunetti, A.-N. Kong, An update on current therapeutic drugs treating COVID-19, Curr. Pharmacol. Rep. (2020) 56–70, https://doi.org/10.1007/s40495-020-00216-7.
[4] S. Elnagdy, M. AlKhazindar, The potential of antimicrobial peptides as an antiviral therapy against COVID-19, ACS Pharmacol. Transl. Sci. (2020) 780–782, https://doi.org/10.1021/acsptsci.0c00059.
[5] L.R. Pizzolato-Cezar, N.M. Okuda-Shinagawa, M.T. Machini, Combinatory therapy antimicrobial peptide-antibiotic to minimize the ongoing rise of resistance, Front. Microbiol. 10 (2019), https://doi.org/10.3389/fmicb.2019.01703.
[6] Q. Wu, J. Patočka, K. Kuča, Insect antimicrobial peptides, a mini review, Toxins 10 (2018) 461, https://doi.org/10.3390/toxins10110461.
[7] D. Phoenix, S.R. Dennison, F. Harris, Antimicrobial Peptides, Wiley-VCH, Weinheim, 2013.
[8] D. Drider, S. Rebuffat (Eds.), Prokaryotic Antimicrobial Peptides, Springer New York, New York, NY, 2011, https://doi.org/10.1007/978-1-4419-7692-5.
[9] G. Wang, X. Li, Z. Wang, APD3: the antimicrobial peptide database as a tool for research and education, Nucleic Acids Res. 44 (2016) D1087–D1093, https://doi.org/10.1093/nar/gkv1278.
[10] A.J. Mason, A. Marquette, B. Bechinger, Zwitterionic phospholipids and sterols modulate antimicrobial peptide-induced membrane destabilization, Biophys. J. 93 (2007) 4289–4299, https://doi.org/10.1529/biophysj.107.116681.
[11] K.A. Brogden, Antimicrobial peptides: pore formers or metabolic inhibitors in bacteria? Nat. Rev. Microbiol. 3 (2005) 238–250, https://doi.org/10.1038/nrmicro1098.
[12] N. Raheem, S.K. Straus, Mechanisms of Action for antimicrobial peptides with antibacterial and antibiofilm functions, Front. Microbiol. 10 (2019), https://doi.org/10.3389/fmicb.2019.02866.
[13] M.-A. Sani, F. Separovic, How membrane-active peptides get into lipid membranes, Acc. Chem. Res. 49 (2016) 1130–1138, https://doi.org/10.1021/acs.accounts.6b00074.
[14] J. Lee, D.G. Lee, Antimicrobial peptides (amps) with dual mechanisms: membrane disruption and apoptosis, J. Microbiol. Biotechnol. 25 (2015) 759–764, https://doi.org/10.4014/jmb.1411.11058.
[15] P.R.S. Sanches, B.M. Carneiro, M.N. Batista, A.C.S. Braga, E.N. Lorenzón, P. Rahal, E.M. Cilli, A conjugate of the lytic peptide Hecate and gallic acid: structure, activity against cervical cancer, and toxicity, Amino Acids 47 (2015) 1433–1443, https://doi.org/10.1007/s00726-015-1980-7.
[16] H. Choi, J.-S. Hwang, D.G. Lee, Coprisin exerts antibacterial effects by inducing apoptosis-like death in *Escherichia coli*, IUBMB Life 68 (2016) 72–78, https://doi.org/10.1002/iub.1463.
[17] F.H. Waghu, S. Joseph, S. Ghawali, E.A. Martis, T. Madan, K.V. Venkatesh, S. Idicula-Thomas, Designing antibacterial peptides with enhanced killing kinetics, Front. Microbiol. 9 (2018), https://doi.org/10.3389/fmicb.2018.00325.
[18] M.S. Castro, T.C.G. Ferreira, E.M. Cilli, E. Crusca, M.J.S. Mendes-Giannini, A. Sebben, C.A.O. Ricart, M.V. Sousa, W. Fontes, Hylin a1, the first cytolytic peptide isolated from the arboreal South American frog *Hypsiboas albopunctatus* ("spotted treefrog"), Peptides 30 (2009) 291–296, https://doi.org/10.1016/j.peptides.2008.11.003.
[19] E. Crusca, A.A. Rezende, R. Marchetto, M.J.S. Mendes-Giannini, W. Fontes, M. S. Castro, E.M. Cilli, Influence of N-terminus modifications on the biological activity, membrane interaction, and secondary structure of the antimicrobial peptide hylin-a1, Biopolymers 96 (2011) 41–48, https://doi.org/10.1002/bip.21454.
[20] B.R. da Silva, V.A.A. de Freitas, V.A. Carneiro, F.V.S. Arruda, E.N. Lorenzón, A.S. W. de Aguiar, E.M. Cilli, B.S. Cavada, E.H. Teixeira, Antimicrobial activity of the synthetic peptide Lys-a1 against oral *streptococci*, Peptides 42 (2013) 78–83, https://doi.org/10.1016/j.peptides.2012.12.001.
[21] R.N. Inui Kishi, D. Stach-Machado, J. de L. Singulani, C.T. dos Santos, A.M. Fusco-Almeida, E.M. Cilli, J. Freitas-Astúa, S.C. Picchi, M.A. Machado, Evaluation of cytotoxicity features of antimicrobial peptides with potential to control bacterial diseases of citrus, PloS One 13 (2018), e0203451, https://doi.org/10.1371/journal.pone.0203451.
[22] E. Crusca, A.S. Câmara, C.O. Matos, R. Marchetto, E.M. Cilli, L.M. Lião, A. Lima de Oliveira, NMR structures and molecular dynamics simulation of hylin-a1 peptide analogs interacting with micelles, J. Pept. Sci. 23 (2017) 421–430, https://doi.org/10.1002/psc.3002.
[23] T.A. Enoki, I. Moreira-Silva, E.N. Lorenzon, E.M. Cilli, K.R. Perez, K.A. Riske, M. T. Lamy, Antimicrobial peptide K^0-W^6-Hya1 induces stable structurally modified lipid domains in anionic membranes, Langmuir 34 (2018) 2014–2025, https://doi.org/10.1021/acs.langmuir.7b03408.
[24] D. Marsh, Handbook of Lipid Bilayers, second ed., CRC Press, Taylor & Francis Group, Boca Raton, FL, 2013.
[25] S. Ohki, Cell and Model Membrane Interactions, Springer, New York, 1991. http://public.ebookcentral.proquest.com/choice/publicfullrecord.aspx?p=3081431. (Accessed 13 July 2020).
[26] G. Rouser, A.N. Siakotos, S. Fleischer, Quantitative analysis of phospholipids by thin-layer chromatography and phosphorus analysis of spots, Lipids 1 (1966) 85–86, https://doi.org/10.1007/BF02668129.
[27] L.R. Gouvea, D.A. Martins, D. da Gama Jean Batista, M. de Nazaré, C. Soeiro, S.R. W. Louro, P.J.S. Barbeira, L.R. Teixeira, Norfloxacin Zn(II)-based complexes: acid base ionization constant determination, DNA and albumin binding properties and the biological effect against *Trypanosoma cruzi*, Biometals 26 (2013) 813–825, https://doi.org/10.1007/s10534-013-9661-z.
[28] J. Marmur, A procedure for the isolation of deoxyribonucleic acid from micro-organisms, J. Mol. Biol. 3 (1961), https://doi.org/10.1016/S0022-2836(61)80047-8, 208-IN1.
[29] J.R. Lakowicz (Ed.), Principles of Fluorescence Spectroscopy, Springer US, Boston, MA, 2006, https://doi.org/10.1007/978-0-387-46312-4.
[30] B. Valeur, Molecular Fluorescence: Principles and Applications, Wiley-VCH, Weinheim ; New York, 2002.
[31] C.C. Vequi-Suplicy, K. Coutinho, M.T. Lamy, New insights on the fluorescent emission spectra of prodan and laurdan, J. Fluoresc. 25 (2015) 621–629, https://doi.org/10.1007/s10895-015-1545-x.
[32] B. Alberts (Ed.), Molecular Biology of the Cell, fifth ed., Garland Science, New York, 2008.
[33] T. Heimburg, Thermal Biophysics of Membranes, Wiley-VCH Verlag, Weinheim, 2007.
[34] G. Denisov, S. Wanaski, P. Luan, M. Glaser, S. McLaughlin, Binding of basic peptides to membranes produces lateral domains enriched in the acidic lipids phosphatidylserine and phosphatidylinositol 4,5-bisphosphate: an electrostatic model and experimental results, Biophys. J. 74 (1998) 731–744, https://doi.org/10.1016/S0006-3495(98)73998-0.
[35] E. Prenner, M. Chiu, Differential scanning calorimetry: an invaluable tool for a detailed thermodynamic characterization of macromolecules and their interactions, J. Pharm. BioAllied Sci. 3 (2011) 39, https://doi.org/10.4103/0975-7406.76463.
[36] K.A. Riske, R.P. Barroso, C.C. Vequi-Suplicy, R. Germano, V.B. Henriques, M. T. Lamy, Lipid bilayer pre-transition as the beginning of the melting process, Biochim. Biophys. Acta BBA - Biomembr. 1788 (2009) 954–963, https://doi.org/10.1016/j.bbamem.2009.01.007.
[37] J. Sun, Y. Xia, D. Li, Q. Du, D. Liang, Relationship between peptide structure and antimicrobial activity as studied by de novo designed peptides, Biochim. Biophys. Acta BBA - Biomembr. 1838 (2014) 2985–2993, https://doi.org/10.1016/j.bbamem.2014.08.018.
[38] P.F. Almeida, A. Pokorny, Antimicrobial peptides, chapter 11, binding and permeabilization of model membranes by amphipathic peptides, in: A. Giuliani, A. C. Rinaldi (Eds.), Antimicrobial Peptides, Humana Press, Totowa, NJ, 2010, https://doi.org/10.1007/978-1-60761-594-1.
[39] S.G. Hovakeemian, R. Liu, S.H. Gellman, H. Heerklotz, Correlating antimicrobial activity and model membrane leakage induced by nylon-3 polymers and detergents, Soft Matter 11 (2015) 6840–6851, https://doi.org/10.1039/C5SM01521A.
[40] A.S. Vasilchenko, E.A. Rogozhin, Sub-inhibitory effects of antimicrobial peptides, Front. Microbiol. 10 (2019), https://doi.org/10.3389/fmicb.2019.01160.
[41] C.-F. Le, C.-M. Fang, S.D. Sekaran, Intracellular targeting mechanisms by antimicrobial peptides, Antimicrob. Agents Chemother. 61 (2017), https://doi.org/10.1128/AAC.02340-16.
[42] J. Yan, K. Wang, W. Dang, R. Chen, J. Xie, B. Zhang, J. Song, R. Wang, Two hits are better than one: membrane-active and DNA binding-related double-action mechanism of NK-18, a novel antimicrobial peptide derived from mammalian NK-Lysin, Antimicrob. Agents Chemother. 57 (2013) 220–228, https://doi.org/10.1128/AAC.01619-12.

[43] R. Eckel, R. Ros, A. Ros, S.D. Wilking, N. Sewald, D. Anselmetti, Identification of binding mechanisms in single molecule–DNA complexes, Biophys. J. 85 (2003) 1968–1973, https://doi.org/10.1016/S0006-3495(03)74624-4.
[44] L. Strekowski, B. Wilson, Noncovalent interactions with DNA: an overview, Mutat. Res. Mol. Mech. Mutagen. 623 (2007) 3–13, https://doi.org/10.1016/j.mrfmmm.2007.03.008.
[45] X. Bi, C. Wang, W. Dong, W. Zhu, D. Shang, Antimicrobial properties and interaction of two Trp-substituted cationic antimicrobial peptides with a lipid bilayer, J. Antibiot. (Tokyo) 67 (2014) 361–368, https://doi.org/10.1038/ja.2014.4.
[46] D.M. Pahlke, U. Diederichsen, Synthesis and characterization of β -peptide helices as transmembrane domains in lipid model membranes, J. Pept. Sci. 22 (2016) 636–641, https://doi.org/10.1002/psc.2912.
[47] D. Zweytick, B. Japelj, E. Mileykovskaya, M. Zorko, W. Dowhan, S.E. Blondelle, S. Riedl, R. Jerala, K. Lohner, N-acylated peptides derived from human lactoferricin perturb organization of cardiolipin and phosphatidylethanolamine in cell membranes and induce defects in *Escherichia coli* cell division, PloS One 9 (2014), e90228, https://doi.org/10.1371/journal.pone.0090228.
[48] N.G. Park, U. Silphaduang, H.S. Moon, J.-K. Seo, J. Corrales, E.J. Noga, Structure−activity relationships of Piscidin 4, a piscine antimicrobial peptide, Biochemistry 50 (2011) 3288–3299, https://doi.org/10.1021/bi101395j.
[49] B. Bechinger, The structure, dynamics and orientation of antimicrobial peptides in membranes by multidimensional solid-state NMR spectroscopy, Biochim. Biophys. Acta BBA - Biomembr. 1462 (1999) 157–183, https://doi.org/10.1016/S0005-2736(99)00205-9.
[50] M.-A. Sani, E. Gagne, J.D. Gehman, T.C. Whitwell, F. Separovic, Dye-release assay for investigation of antimicrobial peptide activity in a competitive lipid environment, Eur. Biophys. J. 43 (2014) 445–450, https://doi.org/10.1007/s00249-014-0970-0.
[51] P. Bhattacharya, S. Mukherjee, S.M. Mandal, Fluoroquinolone antibiotics show genotoxic effect through DNA-binding and oxidative damage, Spectrochim. Acta. A. Mol. Biomol. Spectrosc. 227 (2020) 117634, https://doi.org/10.1016/j.saa.2019.117634.
[52] T. Yi, Y. Huang, Y. Chen, Production of an antimicrobial peptide AN5-1 in *Escherichia coli* and its dual mechanisms against bacteria, Chem. Biol. Drug Des. 85 (2015) 598–607, https://doi.org/10.1111/cbdd.12449.
[53] M. Zampakou, M. Akrivou, E.G. Andreadou, C.P. Raptopoulou, V. Psycharis, A. A. Pantazaki, G. Psomas, Structure, antimicrobial activity, DNA- and albumin-binding of manganese(II) complexes with the quinolone antimicrobial agents oxolinic acid and enrofloxacin, J. Inorg. Biochem. 121 (2013) 88–99, https://doi.org/10.1016/j.jinorgbio.2012.12.013.
[54] J.C. Wang, DNA topoisomerases, Annu. Rev. Biochem. 65 (1996) 635–692, https://doi.org/10.1146/annurev.bi.65.070196.003223.
[55] L. Ma, X. Xie, H. Liu, Y. Huang, H. Wu, M. Jiang, P. Xu, X. Ye, C. Zhou, Potent antibacterial activity of MSI-1 derived from the magainin 2 peptide against drug-resistant bacteria, Theranostics 10 (2020) 1373–1390, https://doi.org/10.7150/thno.39157.
[56] W. Dong, X. Luo, Y. Sun, Y. Li, C. Wang, Y. Guan, D. Shang, Binding properties of DNA and antimicrobial peptide Chensinin-1b containing lipophilic alkyl tails, J. Fluoresc. 30 (2020) 131–142, https://doi.org/10.1007/s10895-019-02478-x.
[57] S. Biswas, S. Samui, A. Chakraborty, S. Biswas, D. De, U. Ghosh, A.K. Das, J. Naskar, Insight into the binding of a non-toxic, self-assembling aromatic tripeptide with ct-DNA: spectroscopic and viscositic studies, Biochem. Biophys. Rep. 11 (2017) 112–118, https://doi.org/10.1016/j.bbrep.2017.07.001.
[58] C.B. Park, H.S. Kim, S.C. Kim, Mechanism of action of the antimicrobial peptide Buforin II: buforin II kills microorganisms by penetrating the cell membrane and inhibiting cellular functions, Biochem. Biophys. Res. Commun. 244 (1998) 253–257, https://doi.org/10.1006/bbrc.1998.8159.
[59] C.-H. Hsu, Structural and DNA-binding studies on the bovine antimicrobial peptide, indolicidin: evidence for multiple conformations involved in binding to membranes and DNA, Nucleic Acids Res. 33 (2005) 4053–4064, https://doi.org/10.1093/nar/gki725.